FOREX Publication
Open Access | Rapid and quality publishing
International Journal of Electrical and Electronics Research (IJEER)
Research Article | Volume 13, Issue 3 | Pages 438-446 | e-ISSN: 2347-470X

Sustainable Grid Integration of PV Systems using Dual-Phase Boost Converter and Intelligent MPPT Techniques

Blessy A. Rahiman[1*], J. Jayakumar[2], and R. Meenal[3]

[1]*Department of Electrical and Electronics Engineering, Karunya Institute of Technology and Sciences, Coimbatore, India; Email: blessynaz@gmail.com*
[2]*Department of Electrical and Electronics Engineering, Karunya Institute of Technology and Sciences, Coimbatore, India; jayakumar@karunya.edu*
[3]*Department of Electrical and Electronics Engineering, V. S. B. Engineering College, Karur, India; meenasekar5@gmail.com*

***Correspondence:** *blessynaz@gmail.com*

ABSTRACT- The increasing demand for energy and environmental concerns necessitate the integration of Renewable Energy Sources (RES), particularly Photovoltaic (PV) systems, into modern power grids. This paper presents an efficient grid connected PV system utilizing a dual-phase Interleaved Boost Converter (IBC) and an intelligent Maximum Power Point Tracking (MPPT) approach based on Adaptive Neuro Fuzzy Inference System (ANFIS). To enhance the controller's performance, optimization algorithms Class Topper Optimization (CTO), Falcon Optimization Algorithm (FOA), and Pufferfish Optimization Algorithm (POA) are employed. The dual phase IBC ensures reduced ripple, improved voltage gain, and stable power conversion. Simulation results in MATLAB/Simulink demonstrate that the proposed system achieves 94% efficiency, 0.95% Total Harmonic Distortion (THD), and a maximum MPPT tracking efficiency of 97.05% using the POA-ANFIS controller.

Keywords: Grid tied PV system, dual phase IBC, ANFIS, MPPT, CTO, FOA, and POA.

ARTICLE INFORMATION

Author(s): Blessy A. Rahiman, J. Jayakumar, and R. Meenal;
Received:09/04/25; **Accepted:** 26/06/25; **Published:** 30/08/25;
E- ISSN: 2347-470X;
Paper Id: IJEER 0904-13;
Citation: 10.37391/ijeer.130307
Webpage-link:
https://ijeer.forexjournal.co.in/archive/volume-13/ijeer-130307.html

Crossref member

Publisher's Note: FOREX Publication stays neutral with regard to jurisdictional claims in Published maps and institutional affiliations.

1. INTRODUCTION

During a period of peak electricity use, the centralized power system is under a significant amount of strain. Significant losses in transmission and distribution lines reduce grid's efficiency [1]. Grid experiences power interruptions for both non-environmental (such as equipment failure) and environmental (such as severe wind or rain) reasons. India's major central power stations typically burn fossil fuels, releasing about 1.026 billion tons of CO2 into the atmosphere annually [2]. Furthermore, a sizable section of India's rural populace lacks access to a dependable power source, which impedes the socioeconomic advancement of the local populace. Renewable energy sources are required as answers to these problems [3] and nation with enormous potential for producing electricity through solar energy.

PV cells and converters with power electronics together comprise a solar energy conversion system [4]. This system is either freestanding or grid connected, depending on the grid's availability. Battery storage is necessary for standalone solar PV systems, raising their initial and ongoing expenses [5][6]. Because grid interfaced solar PV systems not need battery storage, which is more desirable. The energy attained from the PV is low for boosting the power converter is required [7]. To increase the voltage, there are three basic types of converters: Buck, Boost, and Buck-Boost.

The buck converter quickly switches transistors, diode, and other energy storage components to control output voltage. In any case, Converter components experience increased thermal stress as a result of the motor's increasing current levels. [8]. Boost converter ignores the parasitic characteristics and achieves unlimited voltage gain with excessive duty cycle. Nevertheless, in real-world situations, the high duty cycles result in an insufficient need for output voltage, which causes the switches to stay in place for longer [9]. Further, an important source of power management for sustaining steady DC voltage, which is required for different vehicles, is the DC buck-boost converter. Device is less appropriate for high powered EV systems, nevertheless, due to their inability to increase the output voltage ripple and offer galvanic isolation between the input and output [10][11]. The proposed single phase interleaved boost converter overcomes these limitations.

MPPT technique extract the power of solar PV array at its maximum rating. Several ANFIS based algorithm of MPPT controller able to eliminate the error and its parameters are gets tuned by using optimization algorithm. Particle Swarm Optimization (PSO) technique, is population-based search

FOREX Publication
Open Access | Rapid and quality publishing
International Journal of
Electrical and Electronics Research (IJEER)
Research Article | Volume 13, Issue 3 | Pages 438-446 | e-ISSN: 2347-470X

technique that identifies potential solutions by classifying each individual as a particle. It becomes complex while providing optimal tuning parameters as it requires multiple iterations [12]. A unique optimization technique is the Grey Wolf Optimizer (GWO). It displays possible optimization capabilities and follows the wolf hierarchy. However, as it only uses one optimization approach, it performs poorly [13]. To address these drawbacks, CTO, FOA, POA is used. The contribution of the proposed work is

- In order to increase the PV system's output voltage, a dual phase IBC is proposed.

To attain optimal performances, CTO, FOA, POA approaches is integrated for effectively tuning the parameters of ANFIS controller.

2. PROPOSED SYSTEM DESCRIPTION

The diagram depicts a PV grid connected system that efficiently converts solar energy into usable grid power. The PV array generates a DC output voltage (V_{PV}) and current (I_{PV}), which are fed into a dual phase interleaved boost converter. This converter boosts the DC voltage (V_{DC}) while minimizing current ripple and enhancing efficiency. An MPPT controller controls the converter. Which utilizes advanced algorithms such as CTO-ANFIS, FOA-ANFIS and POA-ANFIS to ensure the PV system runs at its peak power by optimizing V_{PV} and I_{PV}, as shown in *figure 1*.

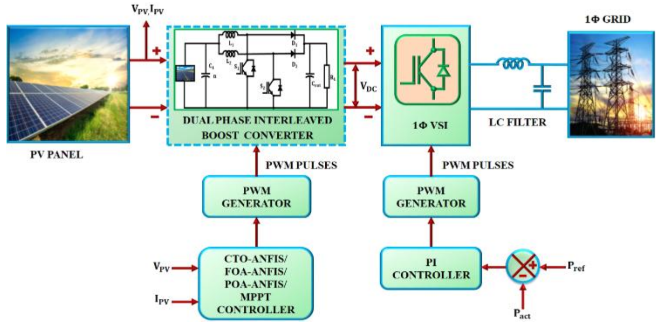

Figure 2. Block diagram of the proposed work

Boosted DC voltage is passed to single phase VSI, which converts it into AC power for grid connection. The inverter is regulated by a PI controller that compares the actual power (P_{act}) with the reference power (P_{ref}) and adjusts the PWM generator to maintain synchronization with the grid. Finally, the AC power is supplied to the single-phase grid, ensuring efficient and stable energy integration.

3. PROPOSED SYSTEM MODELLING

3.1. PV Cell modelling

PV modules widely used to convert light energy into electrical energy in industrial applications. PV cells coupled in series and parallel to boost the output voltage over a single PV cell. Specifically, the module consists of solar cells connected in parallel with (N_P) and in series with (N_S). *Eq. (1)* expresses the PV module's total output current. *Figure 2* below displays the PV module's corresponding circuit.

$$I_L = I_{ph}N_p - I_{01}N_p exp\left[\frac{q\left(V_L+\frac{I_L R_S N_S}{N_P}\right)}{nN_S KT} - 1\right] - \frac{\left(V_L+\frac{I_L R_S N_S}{N_P}\right)}{\frac{R_{sh}N_S}{N_P}} \quad (1)$$

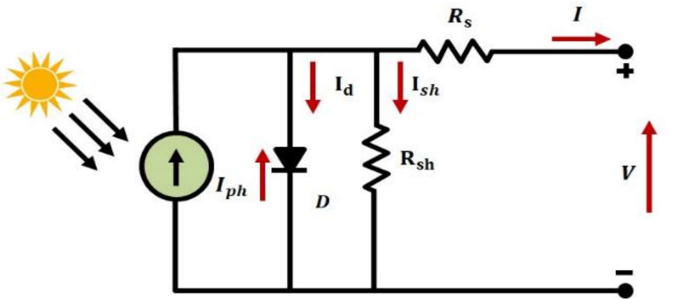

Figure 2. PV module equivalent circuit

Since PV cell typically linked in series, number of PV cells connected in parallel (N_P) is assumed to be 1, enabling the PV module's output current eq. to be expressed as follows,

$$I_L = I_{ph}N_p - I_{01}N_p exp\left[\frac{q\left(V_L+\frac{I_L R_S N_S}{N_P}\right)}{nN_S KT} - 1\right] - \frac{(V_L+I_L R_S N_S)}{R_{sh}N_S} \quad (2)$$

From the PV module, the following parameters need to be estimated as (I_{ph}, I_{01}. R_{sh}, R_S, n). Due to low voltage of PV panels, dual phase interleaved boost converter is used to boost the voltage.

3.2. Dual phase Interleaved Boost Converter (IBC)

The proposed dual phase IBC enhances input voltage, reduces ripple currents, and minimizes copper and conduction losses by splitting the output current into two paths. During operation, switches (S_1) and (S_2) alternately store energy in inductors (L_1) and (L_2), which is then delivered to the load via diodes. This interleaved topology doubles the ripple frequency compared to a single-phase boost converter, ensuring balanced operation with (180^0) phase difference between gate signals, determined by ($360^0/n$), where (n) is the number of phases.

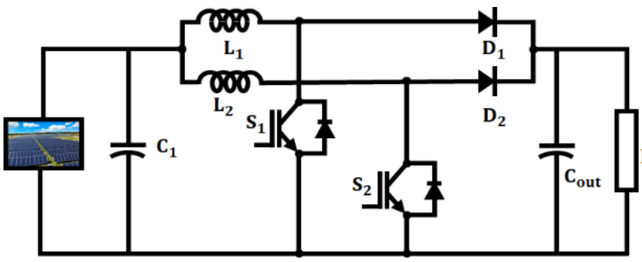

Figure 3. Dual phase interleaved boost converter

The converter theoretical waveforms are depicted in *figure 3*, which shows the outputs and operation modes according to duty cycle (d). The switching positions of (S_1) and (S_2) dictate the four modes of operation of the circuit.

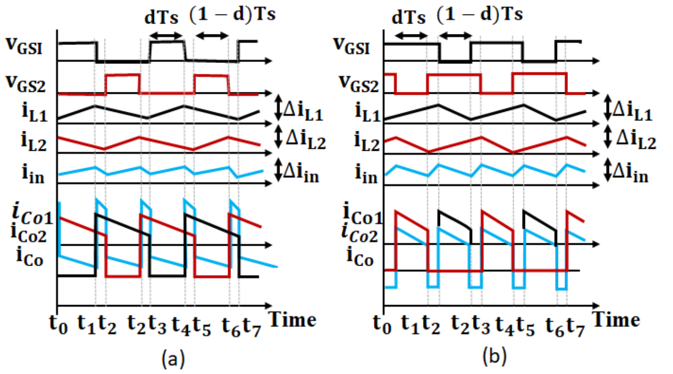

Figure 4. Dual phase IBC waveforms: (a) d ≤ 0.5; (b) d > 0.5

In all modes, as seen in *fig 4(a)*, using zero ripple in output capacitor current, IBC achieves ripple cancellation and reduces input current ripple. The inductors' rising time over time is reflected in the input current's rising slope. (dT_s) for $(d < 0.5)$. The input current ripple rate and peak to peak ripple are calculated using *eq.s (1)* and *(2).*

$$K_{in} = K_{on} - K_{off} = \frac{V_{in}}{L_{in}} - \frac{(V_{out} - V_{in})}{L_{in}} \quad (3)$$

$$\Delta I_{in} = K_{in} d T_s \quad (4)$$

By replacing the input voltage from *eq. (4)* with boost converter's output voltage from *eq. (5)*, input ripple current for $(d < 0.5)$ found, yielding the expression in *eq. (6)*.

$$\frac{V_{out}}{V_{in}} = \frac{1}{1-d} \quad (5)$$

$$\Delta I_{in} = d(1-2d)\frac{V_{out}T_s}{L_{in}} \quad (6)$$

Eq. (8) is used to compute the increasing slope time of the input current is more than $0.5(d < 0.5)$, and *eq. (9)* is used to determine the input current itself.

$$t_{on} = \frac{T_S}{2} - (1-d)T_s \quad (7)$$

$$K_{in} = 2k_{on} = 2\frac{V_{in}}{L_{in}} \quad (8)$$

$$\Delta i_{in} = K_{in}\left(d - \frac{1}{2}\right)T_s = \left(d - \frac{1}{2}\right)(2-2d)\frac{V_{out}T_s}{L_{in}} \quad (9)$$

The following describes the state-space eq.s and operation modes as seen *fig 5*.

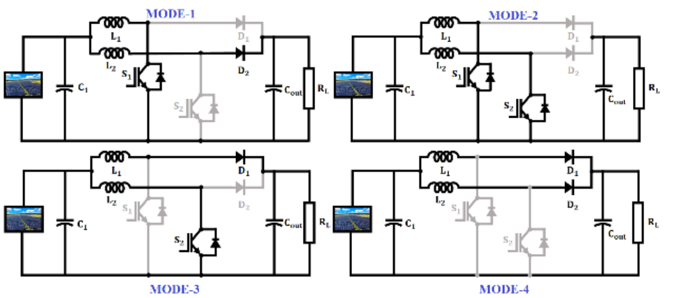

Fig 5. Operating Modes of dual phase IBC

Mode 1: $[t_0 \le t < t_1]$: In the operation mode shown in *figure 4(a)*, with (S_1) on and (S_2) off, inductor (L_1) (IL_1) stores energy as its current increases, resulting in reverse-biasing of the diode in its path.

$$\begin{bmatrix} \frac{di_{L1}}{dt} \\ \frac{di_{L2}}{dt} \\ \frac{dv_0}{dt} \end{bmatrix} = \begin{bmatrix} 0 & 0 & 0 \\ 0 & 0 & -\frac{1}{L_2} \\ 0 & \frac{1}{C_{out}} & -\frac{1}{R_L C_{out}} \end{bmatrix} \begin{bmatrix} i_{L1} \\ i_{L2} \\ v_0 \end{bmatrix} + \begin{bmatrix} \frac{1}{L1} \\ \frac{1}{L2} \\ 0 \end{bmatrix} v_{in} \quad (10)$$

Mode 2: $[t_1 \le t < t_2]$: Using both switching devices activated and both diodes reverse-biased, similar circuit for this operating mode is depicted in *figure 4(b)*. The input currents (L_1) and (L_2) are shared by the inductors in this mode, storing energy and producing equal voltages. *Eq. (11)*, which represents the Mode-2 state space model.

$$\begin{bmatrix} \frac{di_{L1}}{dt} \\ \frac{di_{L2}}{dt} \\ \frac{dv_0}{dt} \end{bmatrix} = \begin{bmatrix} 0 & 0 & 0 \\ 0 & 0 & 0 \\ 0 & \frac{1}{C_{out}} & -\frac{1}{R_L C_{out}} \end{bmatrix} \begin{bmatrix} i_{L1} \\ i_{L2} \\ 0 \end{bmatrix} + \begin{bmatrix} \frac{1}{L1} \\ \frac{1}{L2} \\ 0 \end{bmatrix} v_{in} \quad (11)$$

Mode 3: $[t_2 \le t < t_3]$: The comparable circuit in *figure 4(c)* illustrates how this mode of operation supports Mode-1. This mode keeps (S_2) active while turning off (S_1). As the load is supplied via the (L_1) -(D_1) path, the current through the inductor (L_1) (IL_1) diminishes

$$\begin{bmatrix} \frac{di_{L1}}{dt} \\ \frac{di_{L2}}{dt} \\ \frac{dv_0}{dt} \end{bmatrix} = \begin{bmatrix} 0 & 0 & -\frac{1}{L_2} \\ 0 & 0 & 0 \\ \frac{1}{C_{out}} & 0 & -\frac{1}{R_L C_{out}} \end{bmatrix} \begin{bmatrix} i_{L1} \\ i_{L2} \\ v_0 \end{bmatrix} + \begin{bmatrix} \frac{1}{L1} \\ \frac{1}{L2} \\ 0 \end{bmatrix} v_{in} \quad (12)$$

Mode 4: $[t_3 \le t < t_4]$: The corresponding circuit for this mode of operation is depicted in *figure 4(d)*, where the diodes are forward-biased and both (S_1) and (S_2) are off. In this mode, as the load receives the energy stored in the inductors, represented by (R_L), currents through (L_1) and (L_1) decrease. This is exactly the state-space model for Mode-4 is derived.

$$\begin{bmatrix} \frac{di_{L1}}{dt} \\ \frac{di_{L2}}{dt} \\ \frac{dv_0}{dt} \end{bmatrix} = \begin{bmatrix} 0 & 0 & -\frac{1}{L_1} \\ 0 & 0 & -\frac{1}{L_2} \\ \frac{1}{C_{out}} & \frac{1}{C_{out}} & -\frac{1}{R_L C_{out}} \end{bmatrix} \begin{bmatrix} i_{L1} \\ i_{L2} \\ v_0 \end{bmatrix} + \begin{bmatrix} \frac{1}{L1} \\ \frac{1}{L2} \\ 0 \end{bmatrix} v_{in} \quad (13)$$

The minimal output capacitance (C_{Out}) is found using *eq. (14)*, and the crucial values of inductors (L_1) and (L_1) ensure continuous conduction mode operation are determined using *eq. (17)*.

$$L_1 = L_2 = \frac{d(1-d)^2 R_L T_S}{2} \quad (14)$$

Research Article | Volume 13, Issue 3 | Pages 438-446 | e-ISSN: 2347-470X

$$C_{min} = \frac{dV_0 T_S}{V_{RP} R_L} \tag{15}$$

The switching time is represented by (T_S) in this case, and the permitted ripple voltage at the output is indicated by (V_{RP}).

$$M = \frac{V_0}{V_{in}} = \frac{2}{(1-d)} \tag{16}$$

Eq. (16) provides the voltage conversion ratio (M) for the dual phase IBC. This analysis ensures accurate modeling and control for applications requiring controlled voltage conversion. The ANFIS base MPPT controller is used to control the converter.

3.3. ANFIS based MPPT controller

ANFIS is a hybrid intelligent system that blends fuzzy systems and neural networks used to create a control scheme for a freestanding solar PV system. The ANFIS controller trained for MPPT using copious amounts of data produced by these tests.

3.3.1. Class Topper Optimization (CTO)

This study enhances the CTO algorithm by introducing direct instruction from the class topper (CT) and a self-evaluation stage, allowing students to analyze past and present performance. Students learn from their section toppers (ST), while section toppers gather information from class topper, maintaining dual phase learning process. Optimal controller gains are determined by minimizing the objective function, with course weightages represented by randomly initialized student sets, where each gain reflects a student's success in a section, as shown in *fig. 6*.

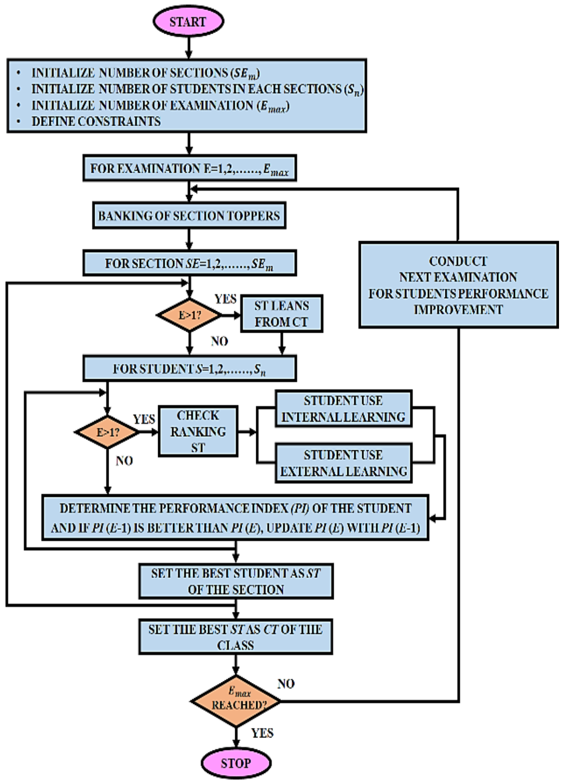

Figure 6. The proposed class topper optimization algorithm's flowchart

The class structure is made up of these sets combined. The following is a definition of the (m) number of sections with n students in each section,

$$SE_{1,2,..m} = \begin{bmatrix} S_1 = [K_p \ T_1 \ T_D \ T_f] \\ \cdots \\ \cdots \\ S_n = [K_p \ T_1 \ T_D \ T_f] \end{bmatrix}_{(n\times1)} \tag{17}$$

The overall performance of student tests the objective function for LFC issue. The objective function 4 used to assess each student's performance in the case of a two-area power system.

$$ITAE_{m,n}^{Emax} = \int_0^{t_{max}} (|\Delta f_1| + |\Delta f_2| + |\Delta P_{tie1-2}| tdt) \tag{18}$$

Student level instruction for the LFC problem:

$$S_{gains^{(S,E+1)}} = S_{gains^{(S,E)}} + I^{(S,E+1)} \tag{19}$$

Where stands for student gains, ST_{gains} for ST gains, and gains for controller parameter.

Section level instruction for the LFC problem:

$$ST_{gains^{(SE,E+1)}} = ST_{gains^{(SE,E)}} + I_1^{(S,E+1)} \tag{20}$$

3.3.2. Falcon optimization algorithm (FOA)

The FOA is novel class of algorithms that draw inspiration from the environment. The falcon's location determined by duty ratio D of DC/DC converter, while PV power is utilized as objective function. The proposed FOA flowchart is shown in *fig. 7*.

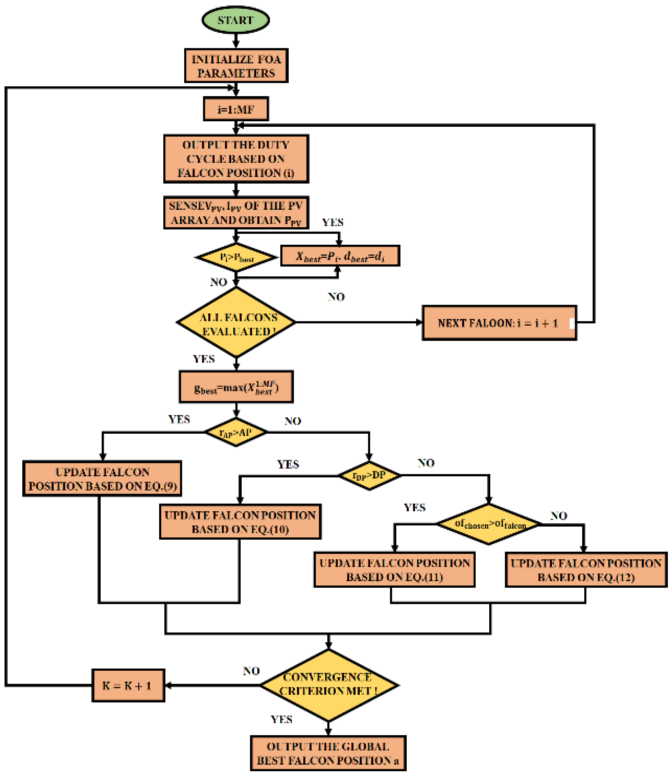

Figure 7. The proposed falcon optimization algorithm's flowchart

FOREX Publication
Open Access | Rapid and quality publishing
International Journal of
Electrical and Electronics Research (IJEER)
Research Article | Volume 13, Issue 3 | Pages 438-446 | e-ISSN: 2347-470X

The following describes the different steps required to apply the FOA approach in an MPPT application:

Step 1: Establish control parameters, set up the starting problem data. The optimization problem, decision variables, and constraints are all outlined.

Step 2: Set falcons' initial position speed. To ensure that the initial distribution of the searching area is equal to each obtaining agent, the following eq. is utilized.

$$d_0^k = \frac{K}{(s_s+1)} \tag{21}$$

Where (s_s) is the swarm's size and d_0^k is the falcon's starting location in the swarm with order k. The max and min values of V are utilized to choose speeds at random are defined as follows.

$$V_{max} = 0.1 \times ub \tag{22}$$

$$V_{min} = -V_{max} \tag{23}$$

Step 3: Evaluate fitness and determine the top ranks for each person and the world.

$$f(d) = maxP_{PV}(d) \tag{24}$$

Step 4: Update the falcon positions and create new ones. In the case where DP exceedsr_{DP}, the chosen prey's fitness is assessed in comparison to the falcon's fitness.

$$X_{iter+1} = X_{iter} + V_{iter} + C_c r(X_{best} - X_{iter}) \tag{25}$$

Step 5: Convergence determination. Once a predefined number of repetitions is finished a predefined threshold optimization process is stopped. To enable it to follow GMPP, duty cycle at which DC/DC converter operates as an output is now used.

3.3.3. Puffer fish Optimization Algorithm (POA)

The next section introduces the Pufferfish Optimization Algorithm (POA), which uses repeated demographic searches to address optimization challenges. Each POA member selects variable values based on its position in the search space, represented as a vector of option variables forming a potential solution. The initial positions of all members in the population are determined using *eq. (26)*.

$$y_{i,d} = LB_d + rand \times (UB_d - LB_d) \tag{26}$$

The process for expressing a collection of analyzed findings into a vector for the problem's objective function is described in *eq. (27)*.

$$F = \begin{bmatrix} F_1 \\ \vdots \\ F_i \\ \vdots \\ F_M \end{bmatrix}_{M\times 1} = \begin{bmatrix} F(Y_1) \\ \vdots \\ F(Y_i) \\ \vdots \\ F(Y_M) \end{bmatrix}_{M\times 1} \tag{27}$$

Where (F_i) is estimated objective function corresponding to i^{th} POA component, and F vector containing estimated objective function.

Phase 1: In the early stages of POA, group members' locations are adjusted by simulating the predatory strategy against the pufferfish, which are slow to predators. After simulating the predator's approach, each POA member's new position in the problem-solving space is determined using *eq. (28)*.

$$Y_{i,j}^{P1} = y_{i,j} + rand_{i,j} \times (SP_{i,j} - J_{i,j} y_{i,j}) \tag{28}$$

Where $(SP_{i,j})$ indicates the pufferfish's j^{th} dimension and (SP_i) indicates the pufferfish selected at random for the i^h predator from the CP_i set. The newly calculated location for the i^{th} predator, as determined by the initial stage of the proposed POA, is indicated by $(Y_i^{P^1})$, while its jth dimension is indicated by $(Y_{i,j}^{P1})$.

Phase 2: By modeling a pufferfish's defense mechanism against predator attacks, population members are moved during the second stage of POA. Therefore, *eq. (29)* indicates that improving the objective function value is a prerequisite for updating each POA member.

$$Y_1 = \begin{cases} Y_i^{P^2} & F_i^{P^2} < F_i \\ Y_i & else \end{cases} \tag{29}$$

Where $(Y_{i,j}^{P^2})$ denotes the predator's jth dimension and $(Y_i^{P^2})$ is the newly calculated location for i^{th} predator obtained from the proposed POA's second phase.

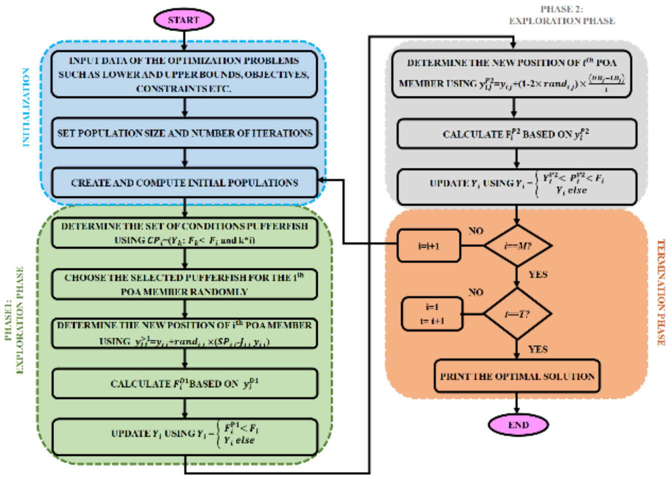

Fig 8. The proposed Puffer fish optimization algorithm flowchart

The first iteration of the POA algorithm concludes once all members' positions are updated during exploration and exploitation phases. After full execution, the top performing POA member is selected as solution. A flowchart illustrating the POA implementation process is shown in *figure 8*. By leveraging POA's capabilities, design of SPV, WT, and grid-based PEV charging stations is continually optimized for sustainability, economy, and efficiency.

Research Article | Volume 13, Issue 3 | Pages 438-446 | e-ISSN: 2347-470X

4. RESULTS AND DISCUSSION

This section reveals the validation outcomes utilizing the developed system with three different optimization algorithms under steady state condition of PV. Followed by *table 1* displays the parameter and its specifications.

Table 1. Parameter and Specification

Parameter	Specification
PV System	
Rated Power	$10kW$
Irradiance	$1000W/m^2$
Temperature	25^0C
No. of panels in Parallel	5
Open circuit Voltage	$37.25V$
Cell linked in Series	36
No. of Panels in series	4
Short Circuit Current	$8.95A$
Dual phase interleaved boost Converter	
L_1, L_2	$4.7\ mH$
Switching frequency	$10KHz$
C_1, C_2, C_{out}	$22\mu F$, $2200\mu F$
Converter efficiency	94%
THD	0.95%

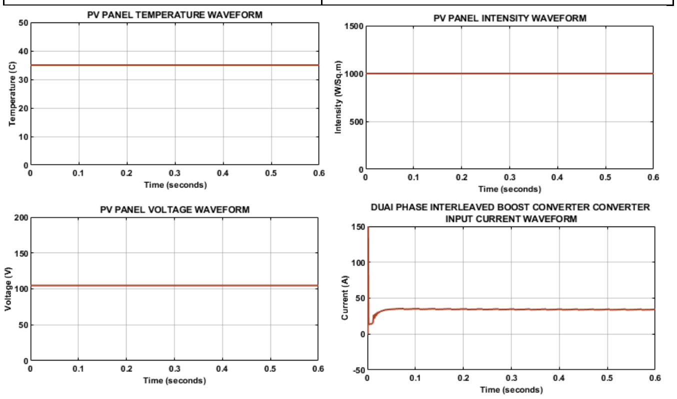

Figure 9. PV at Steady State Condition

The waveform presented in *fig. 9* demonstrates the performance of PV under steady operating condition. It is seen that, the temperature and intensity waveform remain at a constant level by maintaining 25°C and intensity of $1000\ W/m^2$. In this scenario, the PV voltage is noticed to be maintaining at 110V, with current measuring 40A, respectively.

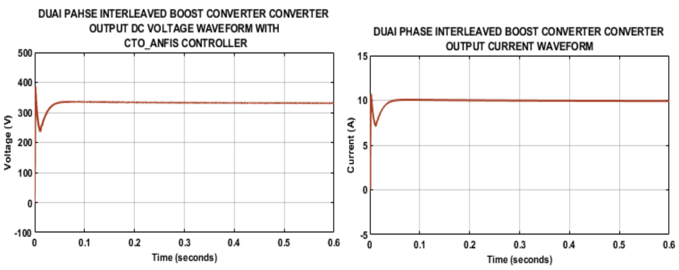

Figure 10. Converter Output using CTO-ANFIS MPPT

The performance of proposed converter utilizing CTO-ANFIS MPPT approach is demonstrated in *fig.10.* It is noticed that, with initial peak rise in voltage a stabilized voltage of 330V is accomplished by the system. In addition, the proposed converter reveals 10A current at certain instances.

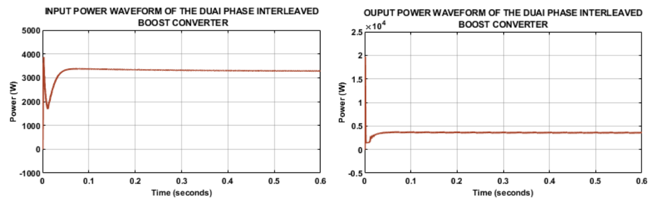

Figure 11. Power Characteristics Waveform using CTO-ANIS MPPT

The power of PV and converter is presented in *fig 11*. The input power continues at 3200 W, whereas the output power maintains at $0.4 \times 10^4 W$, respectively.

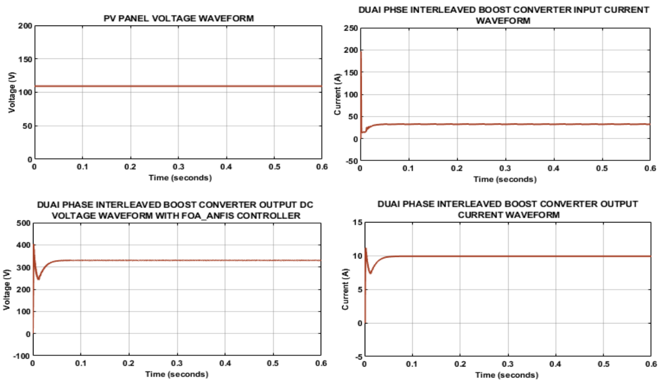

Figure 12. Converter Input/Output using FOA-ANFIS MPPT

Similarly, the converter is tested using FOA-ANFIS MPPT Controller and the corresponding outcomes are presented in *fig.12*. It is to be noticed that, a stabilized voltage of 110V, with current 40A is fed as input to the proposed converter. Utilizing the input the converter response with initial rise in voltage to a peak level of 390V, and stabilizes 330V after certain instance. Meanwhile the current is maintained at 10A with minor oscillations at the beginning.

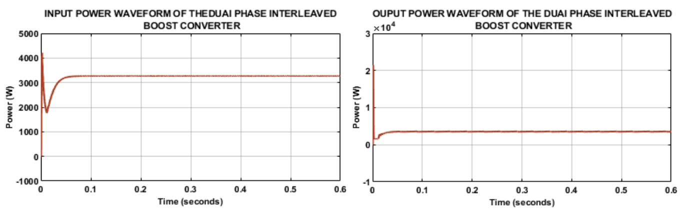

Figure 13. Power Characteristics Using FOA-ANFIS MPPT

Fig. 13 shows the power waveforms of dual phase interleaved boost converter under FOA_ANFIS MPPT. The input power rises and continues at a level of 3100 W, whereas the output power with initial distortion continues at $0.4 \times 10^4 W$.

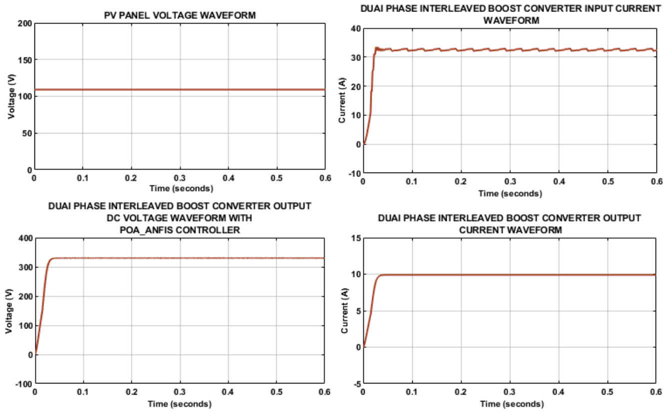

Figure 14. Converter Input/Output Characteristics using POA-ANFIS MPPT

The characteristics of converter utilizing the proposed control strategy is demonstrated in *fig.14*. The input voltage of PV as like in other condition continues at 110V, while the current waveform demonstrates minor oscillations maintaining a current level of 35A, respectively. Depending on the input, the converter reveals boosted voltage of 330V, and a stabilized 10A current.

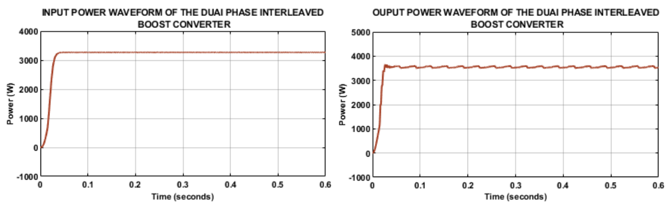

Figure 15. Power Characteristics using POA-ANFIS MPPT

Figure 15 display the characteristic waveform of PV and converter using POA-ANFIS under steady state condition. The input power is maintaining a stabilized power value of 3200W, with output power fluctuating near 3500W, respectively.

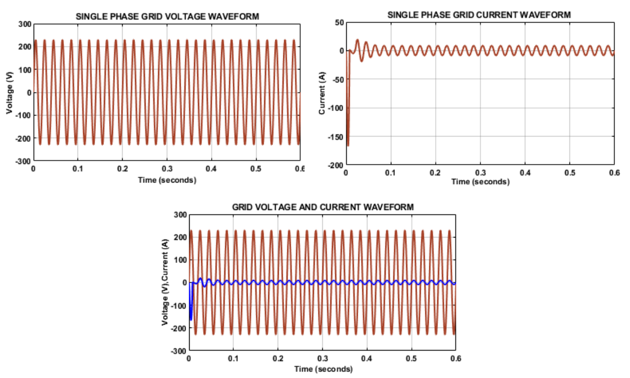

Fig.16. Grid waveform of voltage and current

Figure 16 shows grid performance characteristics, where a grid voltage of 230V, with grid current 8A, is accomplished. Morover, the inphase waveform reveals the effective synchronization of grid.

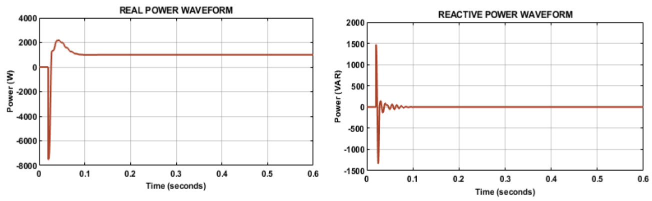

Figure 17. Real and reactive power waveform

Figure 17 illustrates the waveforms of reactive and real power. The reactive power waveform remains stable, indicating consistent reactive power management within the system. Similarly, the real power waveform, which stays constant at 1500 W. This steady real power demonstrates reliable energy delivery, ensuring dependable system operation.

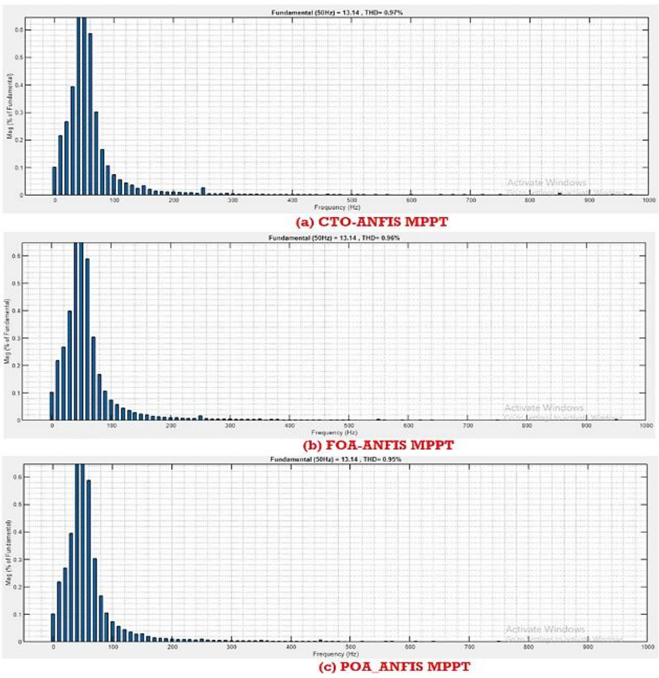

Figure 18. THD Values

The harmonic analysis of grid current utilizing different MPPT controller is presented in *fig.18*. It is seen that, utilizing CTO and FOA-ANFIS 0.97% and 0.96% THD, whereas the proposed POA-ANFIS reveals reduced THD of 0.95%, overcoming CTO and FOA_ANFIS approaches.

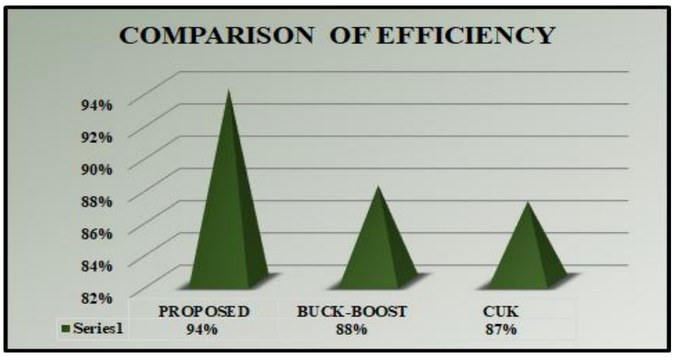

Figure 19. Comparison of efficiency

Figure 19 compares the efficiency of various converters, highlighting the proposed converter achieves highest efficiency at 94%, outperforming Buck Boost converter (88%) [14] and Cuk converter (87%) [15].

Table 2. Comparison of THD

MPPT Techniques	THD (%)
P&O	1.80
Fuzzy Logic	1.76
ANN	1.2
POA-ANFIS	0.95%

The THD analysis of different optimized ANFIS MPPT approach is compared in *table 2*. It is seen that, only minor reduction is noted on all the three control approaches. However, the developed POA-ANFIS tends to ranks with improved THD value of 0.95%, overcoming CTO-ANFIS of 0.97% and FOA-ANFIS of 0.96%, respectively.

Table 3. Performance Metrics

Algorithm	Convergence time	Fitness value	THD%
CTO-ANFIS	0.07	0.023	0.97
FOA-ANFIS	0.06	0.019	0.96
POA-ANFIS	0.04	0.013	0.95

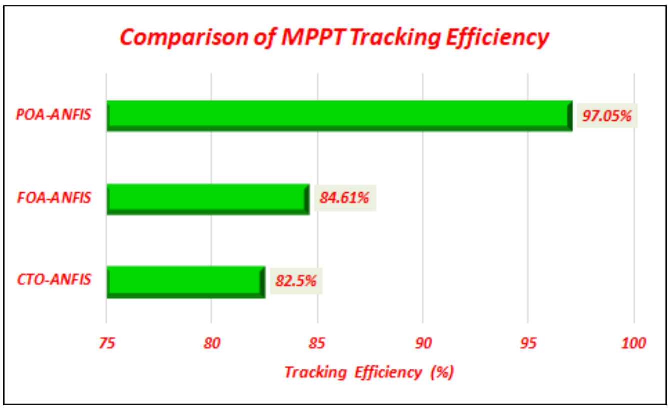

Figure 20. Comparison of MPPT Tracking Efficiency

The assessment of MPPT tracking efficiency utilizing three different optimization algorithm is presented in *fig.20*. It is noted that, using CTO-ANFIS 82.5% is achieved, with FOA-ANFIS it is 84.61% and by the proposed POA-ANFIS it is 97.05% respectively. This reveals that the proposed POA-ANFIS excels in tracking maximum power, when compared to others.

5. CONCLUSIONS

The proposed grid tied PV system, incorporating a dual phase interleaved boost converter and an ANFIS-based MPPT algorithm, offers a highly efficient solution for renewable energy integration. The dual-phase IBC ensures effective DC-DC conversion and stable voltage control. This work integrates three different optimization algorithm based ANFIS MPPT for tracking of maximum power from PV system. Validation after MATLAB reveals that the proposed converter reveals improved converter efficiency of 94%, with improved voltage gain. Comparative analysis reveals that, the POA_ANFIS MPPT demonstrates superior performance with improved tracking efficiency of 97.05% and reduced THD measure of 0.95%, respectively. This highlights that, the proposed research addresses the growing demand for sustainable and reliable renewable energy integration.

REFERENCES

[1] M. Badoni, A. Singh, A. K. Singh, H. Saxena, and R. Kumar, “Grid tied solar PV system with power quality enhancement using adaptive generalized maximum Versoria criterion,” CSEE J. Power Energy Syst., vol. 9, no. 2, pp. 722–732, 2021.

[2] Z. T. Nayyef, M. M. Abdulrahman, and N. A. Kurdi, “Optimizing energy efficiency in smart grids using machine learning algorithms: A case study in electrical engineering,” SHIFRA, vol. 2024, pp. 46–54, Apr. 2024. doi: 10.70470/SHIFRA/2024/006.

[3] Y. Niu, V. Abdullayev, A. V. Alyar, and A. T. Kamran, “Green technologies and their role in mitigating climate change: A comparative study across developing nations,” ESTIDAMAA, vol. 2023, pp. 27–35, Apr. 2023. doi: 10.70470/ESTIDAMAA/2023/004.

[4] V. Abdullayev, Y. Niu, N. Ragimova, A. V. Alyar, and A. T. Kamran, “Harnessing renewable energy for sustainable urban development: Case studies from the MENA region,” ESTIDAMAA, vol. 2023, pp. 9–17, Feb. 2023. doi: 10.70470/ESTIDAMAA/2023/002.

[5] Y. Niu, V. Abdullayev, A. V. Alyar, and A. T. Kamran, “Resilience and adaptation to climate change: Community-based strategies in coastal regions,” ESTIDAMAA, vol. 2023, pp. 36–43, May 2023. doi: 10.70470/ESTIDAMAA/2023/005.

[6] K. Dhibi et al., “Interval-valued reduced ensemble learning based fault detection and diagnosis techniques for uncertain grid-connected PV systems,” IEEE Access, vol. 10, pp. 47673–47686, 2022.

[7] Y. Li, S. Sahoo, T. Dragičević, Y. Zhang, and F. Blaabjerg, “Stability-oriented design of model predictive control for DC/DC boost converter,” IEEE Trans. Ind. Electron., vol. 71, no. 1, pp. 922–932, Jan. 2023.

[8] D. H. Rasheed and S. B. Tambe, “Advancing energy efficiency with smart grids and IoT-based solutions for a sustainable future,” ESTIDAMAA, vol. 2024, pp. 36–42, Apr. 2024. doi: 10.70470/ESTIDAMAA/2024/006.

[9] M. Nivedha, “PV connected grid system using modified boost converter with AI-based controller,” Proc. Int. Conf. on Electrical, Electronics, and Computer Engineering, 2024.

[10] V. Kumar, S. Rattan, S. Prakash, and T. C. Sameer, “Artificial Neural Fuzzy Based MPPT for High Gain Zeta Converter for Standalone PV Application with Galvanic Isolation,” in Proc. IEEE RAEEUCCI, pp. 1–5, 2024.

[11] K. S. Kavin et al., “Improved BRBFNN-based MPPT algorithm for coupled inductor KSK converter for sustainable PV system applications,” Electr. Eng., pp. 1–23, 2025. [Online]. Available: https://link.springer.com/article/10.1007/s00202-025-01732-9.

[12] K. S. Kavin et al., “Coupled inductor interleaved boost converter with ANN and RNN based MPPT algorithm for PV system,” Int. J. Appl. Power Eng., vol. 13, no. 3, pp. xx–xx, 2024.

[13] J. L. Seguel, S. I. Seleme Jr, and L. M. F. Morais, “Comparative study of Buck-Boost, SEPIC, Cuk and Zeta DC-DC converters using different MPPT methods for photovoltaic applications,” Energies, vol. 15, no. 21, p. 7936, 2022.

[14] K. A. Mahafzah et al., "A new Cuk-based DC-DC converter with improved efficiency and lower rated voltage of coupling capacitor," Sustainability, vol. 15, no. 11, p. 8515, 2023. doi: 10.3390/su15118515.

[15] H. Tekin, G. Setrekli, E. Murtulu, H. Karşıyaka, and D. Ertekin, "A proposed single-input multi-output battery-connected DC–DC buck–boost converter for automotive applications," Electronics, vol. 12, no. 20, p. 4381, 2023.